PROBLEMY MECHATRONIKI
UZBROJENIE, LOTNICTWO, INŻYNIERIA BEZPIECZEŃSTWA

ISSN 2081-5891

9, 4 (34), 2018, 113-126

PROBLEMS OF MECHATRONICS
ARMAMENT, AVIATION, SAFETY ENGINEERING

A Digital Model of the Electrodynamic Acceleration Process in a Coil Gun Device

Andrzej W. HORODEŃSKI, Cezary POCHRYBNIAK

National Centre for Nuclear Research
7 Andrzeja Sołtana Str., 05-400 Otwock, Poland
Corresponding author's e-mail address: Cezary.Pochrybniak@ncbj.gov.pl

Received by the editorial staff on 21 February 2018
The reviewed and verified version was received on 10 December 2018

DOI 10.5604/01.3001.0012.7337

Abstract. The subject of this paper is an analysis of the process of applying kinetic energy to a projectile made from a non-magnetic, electrically conductive material and placed inside of an inductance coil live with alternating current. A digital model of an acceleration system was built, comprising a high-current coil and a cylindrical projectile located inside of the coil. Analytical formulas of the three-dimensional distribution of the axial and radial components of the magnetic field generated by the coil were applied [1]. The mathematical model described herein included the projectile and coil three-dimensional system (with the dimensions and distribution of the coil turns), the parameters of the power supply system and their variations, caused by the energy input to the projectile (and including the variation of: coupling coefficient, pulsation, coefficient of attenuation, inductance, and resistance), and the balance of momentum of the projectile and coil system. A system of equations which depicted the projectile and coil system (the law of electromagnetic induction, the Biot-Savart law, electric-to-kinetic energy transfer, and the balance of momentum of the projectile and coil system) was solved with numerical methods.

The conclusions relevant to the design and technology of an ICG (Inductance Coil Gun), derived from the foregoing numerical analysis, were experimentally verified. Initial calculations were completed to optimise the acceleration process. The acceleration efficiency in a cascade of 10 coils was calculated.
Keywords: Coil Gun, acceleration, electromagnetic force, coil, propulsion, electromagnetism

1. BACKGROUND

The subject of this paper is an analysis of the process of kinetic energy input to (or acceleration of) a projectile made from a non-magnetic, electrically conductive material and placed inside of a solenoid coil, powered by a capacitor bank via a low-inductance connection, and a preliminary experimental verification of the analysis results.

Inductance Coil Guns (ICG) have been researched by many research laboratories around the world [2-8] for potential applications as projectile devices or projectile weapons. This paper was stimulated by the lack of a model for electrodynamic acceleration in the reference literature which would consider the variability of the power supply circuit parameters caused by the motion of the projectile as an energy load.

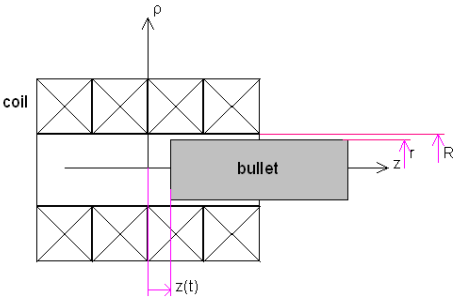

Fig. 1. Schematic diagram of the projectile and coil system

2. ASSUMPTIONS

The distribution of the magnetic fields and forces applied to the projectile was expressed as follows (with cylindrical coordinates):

$$\mathbf{B} = [B_r, B_\varphi, B_z], \qquad \mathbf{J} = [0, I_\varphi, j_z]$$

Coupling the magnetic field with the eddy current resulted in a Lorentz force that acted on the projectile as follows:

$$\mathbf{F} \sim \mathbf{J} \times \mathbf{B}$$

with a variety of components:

$F_z \sim B_r \cdot J_\varphi$ – projectile acceleration;
$F_r \sim B_z \cdot J_\varphi$ – projectile compression;
$F_\varphi \sim B_r \cdot J_z$ – generation of torque.

The analysis of the acceleration process was completed, given the following assumptions:

1. The process was quasi-static: the length of the electromagnetic wave generated by the projectile and coil system was much larger than the size of the system, and thus the process of electromagnetic wave emission was reasonably omitted.
2. $\partial/\partial\theta = 0$ (axial symmetry).
3. The projectile which was accelerated was a cylinder made from a (metallic) electrically conductive material with a known specific resistance, ρ, and devoid of magnetic properties (which meant that its magnetic susceptibility was zero) in the superficial layer, the depth of which was $\sigma = \sqrt{(2\rho/\mu_0\omega)}$.
4. The calculations were completed for a 'mean' coil, i.e. with a single winding layer with a diameter equal to the arithmetic mean of the inner and outer diameter.

3. MAGNETIC FIELD

It was known from the references [1] that the relative distribution values for the radial and axial components of the magnetic field generated by a single thin coil through which current is flowing were expressed with the following formulas:

$$h_{1r}(\rho,\zeta) = \frac{\zeta\left(\left(\zeta^2+\rho^2+1\right)E\left(-\frac{4\rho}{(\rho-1)^2+\zeta^2}\right)-\left(\zeta^2+(\rho+1)^2\right)K\left(-\frac{4\rho}{(\rho-1)^2+\zeta^2}\right)\right)}{2\pi\rho\sqrt{\zeta^2+(\rho-1)^2}\left(\zeta^2+(\rho+1)^2\right)} \tag{1}$$

$$h_{1z}(\rho,\zeta) = \frac{\left(\zeta^2+(\rho+1)^2\right)K\left(-\frac{4\rho}{(\rho-1)^2+\zeta^2}\right)-\left(\zeta^2+\rho^2-1\right)E\left(-\frac{4\rho}{(\rho-1)^2+\zeta^2}\right)}{2\pi\sqrt{\zeta^2+(\rho-1)^2}\left(\zeta^2+(\rho+1)^2\right)} \tag{2}$$

with:
E, K – elliptical integrals;
ρ, ζ – cylindrical coordinates relative to the coil radius, R.

It was easy to generalise the case of the thin coil as a case of an extensive coil with formulas (3 to 6):

$$h_r(\rho,\zeta) = \frac{1}{2a}\int_{-a}^{a} h_{1r}(\rho,\zeta-u)\,du \tag{3}$$

$$h_z(\rho,\zeta) = \frac{1}{2a}\int_{-a}^{a} h_{1z}(\rho,\zeta-u)\,du \tag{4}$$

Assumption 1 allowed the following expression of the magnetic field:

$$B_r(\rho,\zeta) = \frac{\mu_0 n I_1(t)}{R} h_r(\rho,\zeta) \tag{5}$$

$$B_z(\rho,\zeta) = \frac{\mu_0 n I_1(t)}{R} h_z(\rho,\zeta) \tag{6}$$

with:

a – one half of the coil length relative to the coil radius, R;
$I_1(t)$ – coil current;
μ_o – magnetic permeability of vacuum;
n – number of coil turns.

Figure 2 shows the example distribution of the radial and axial components of the magnetic field calculated with these formulas. The plots in Fig. 2 demonstrate that the short coil was the more favourable configuration. All calculations presented herein applied to a coil, the length to inner diameter ratio of which was 1.

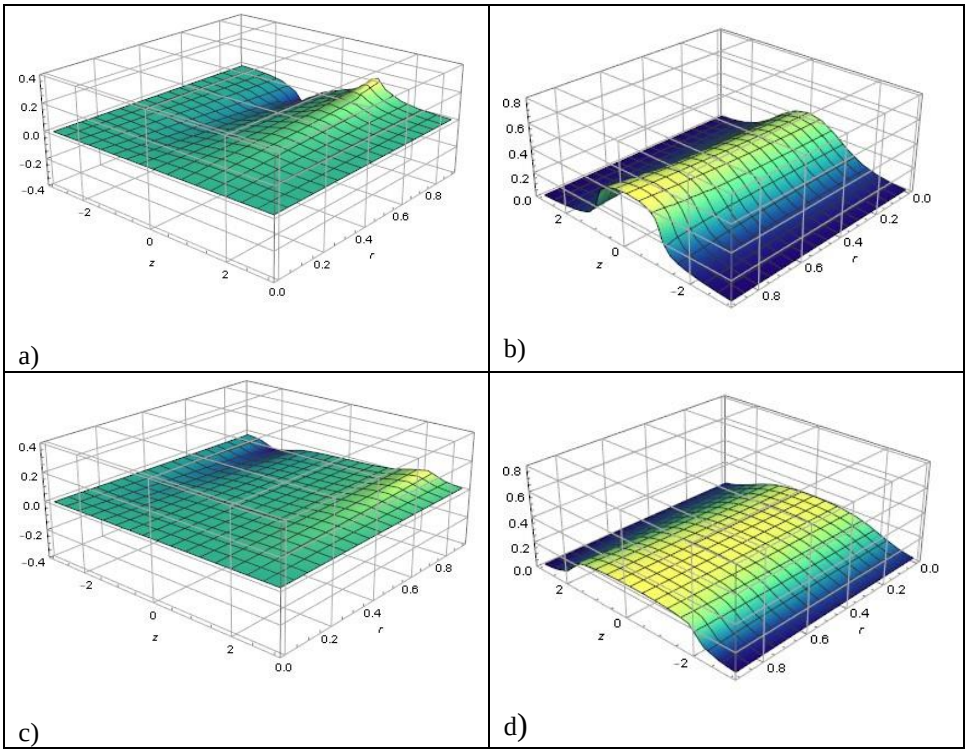

Fig. 2. Examples of the distribution values for the radial component, (a), (c), and the axial component, (b), (d), of the magnetic field along the coil radius for different axial positions in a short coil (length to inner diameter ratio = 1) – see the top row – and in a long coil (length to inner diameter ratio = 2 : 1) – see the bottom row

4. BALANCE OF MOMENTUM

The projectile and coil system was a specific case of two massive bodies, with one of them (the coil) acting on the other (the projectile) according to the conservation of momentum. When the inductance coil pushed the projectile out of the magnetic force effect area, it applied momentum both to the projectile and itself, and the sum of momentums was equal to zero. Hence, the projectile energy's share of the total projectile and coil system energy:

$$\chi = E_{proj}/E_{tot} = \frac{1}{\sqrt{(1+v)}} \tag{7}$$

with: $v = m_{proj}/m_{coil}$

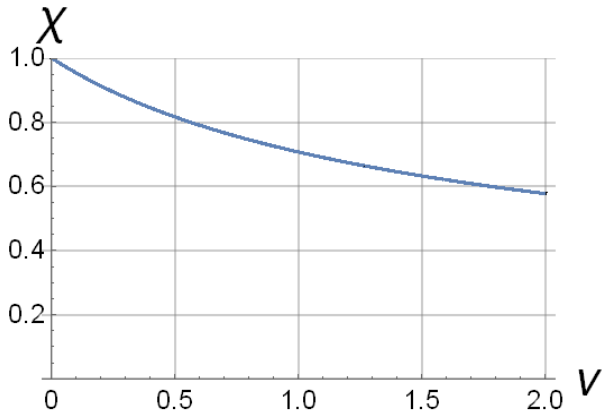

Fig. 3. Share of the projectile energy in the total system energy from the balance of momentums

The projectile and the coil shared the energy inversely to the ratio of their masses. This was significant to the technology of the inductance coil. First, a coil made of thick wire with the maximum feasible wire size (cross-sectional area) had to be used. Second, it was necessary to firmly anchor the coil to its body so that the two parts became the repulsive mass.

It was then necessary to verify the calculation results presented in the previous section. The calculations considered only a case in which the entire momentum is transferred to the projectile. In an attempt to produce a result more approximate to the reality, the expression of projectile velocity, (24), required the measure of $v \cdot \chi$ to replace v.

5. POWER SUPPLY CIRCUIT

The projectile and coil system was a system of coupled inductance that was powered with current from a capacitor bank, see Fig. 4 (above). Here, the secondary circuit was represented by the eddy current generated within the projectile material and flowing along the projectile circumference [9]. For analytical purposes, a simpler substitutive circuit could be used, as shown in Fig. 4 (below).

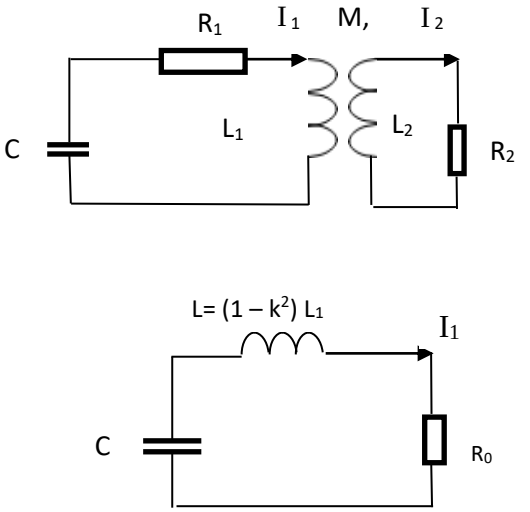

Fig. 4. RLCM system (see above) and the substitute diagram of the coil power supply system (see below)

Given the assumption that $R_0 < 2\sqrt{(L/C)}$ (which was true in the test contemplated herein), the solutions of the circuit were expressed in the following form:

$$U = \frac{Uo}{\cos(\delta)} e^{-\alpha t}(\cos(\omega t+\delta)) \tag{8}$$

$$I_1(t) = I_0 f_1(t) \tag{9}$$

$$I_2(t) = knI_0 f_2(t) \tag{10}$$

with:

$f_1(t) = e^{-\alpha t} \sin(\omega t)$; $f_2(t) = e^{-\alpha t} \sin\left(\omega t - \operatorname{arctg}\left(\frac{\beta-\alpha}{\omega}\right)\right)$; $I_0 = \frac{Uo\ \omega}{\cos(\delta)}$;

$\alpha = R_o/2L_o$; $\omega_0 = 1/\sqrt{(L_oC)}$; $\omega = \sqrt{(\omega_0^2 - \alpha^2)}$; $\delta = -\operatorname{arctg}\left(\frac{\alpha}{\omega}\right)$; $\beta = n^2 R_2/L_1$;

$L_o = (1 - k^2) L_1$

C – energy bank capacity;
R_1, R_2 – primary and secondary side resistance, respectively;
R_o – resultant resistance of the whole circuit, $R_o = R_1 + k^2 n^2 R_2$;
n – number of coil turns;
k – coupling coefficient;
L_o – resultant inductance of the circuit.

The coil inductance was calculated with one of the commonplace empirical formulas:
$L = Dn^2/(l/D+0.45)\cdot 10^{-6}$ [cm, μH]
D – coil diameter (the arithmetic mean of the inner and outer diameter values);
l – coil length; n – number of coil turns.

6. COUPLING COEFFICIENT

The calculations of the parameters of the coil power supply circuit required the knowledge of the coupling coefficient in the projectile and coil system. By definition:

$$k(\zeta) = \Phi_p(\zeta)/\Phi_0 \tag{12}$$

with:
Φ_0, Φ_p – magnetic flux values: the total magnetic flux and the magnetic flux within the projectile's cross-section, respectively.

Formulas (3 to 6) provided the following:

$$k(\zeta) = \frac{\int_0^r \rho\, h_{1z}(\rho,\zeta)\, d\rho}{\int_0^1 \rho\, h_{1z}(\rho,0)\, d\rho} \tag{13}$$

with: r – relative mean radius of the projectile.

As shown in Fig. 5, the coupling coefficient depended on the projectile's location.

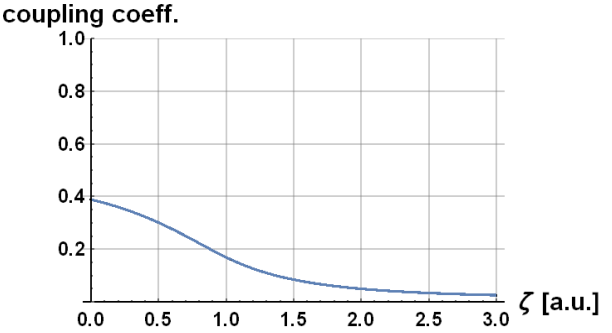

Fig. 5. Relationship of coupling coefficient to the projectile's position in the short coil (l/D = 4/3)

The resultant coupling coefficient, i.e. the representation of the coupling coefficient in the primary side circuit, was a weighted average from distribution (13), where the statistical weight was the axial distribution of current density:

$$k_{eff}(\zeta) = \frac{\int_{\zeta}^{\zeta_{max}} j(r,\xi,t)\, k(\xi)\, d\xi}{\int_{\zeta}^{\zeta_{max}} j(r,\xi,t) d\xi} \tag{14}$$

7. KINETIC RESISTANCE

The process by which the projectile received energy from the power supply circuit was evident in the power supply circuit as a kinetic resistance which was dynamically input to the circuit and varied in time. The kinetic resistance directly affected the time constant of capacitor discharge, α, which in turn was a major contributor to the energy balance of the process, and the ultimate result of the calculations. The distribution of energy in every electrical system depends on the resistance values present. It was sufficient to determine the kinetic resistance value by comparing the expressions for the projectile kinetic energy increase to the energy released by the power supply circuit at resistance R_{kin}:

$$mv \cdot dv = I(t)^2 R_{kin} dt \tag{15}$$

with: v – velocity of the projectile.

Hence:

$$R_{kin} = \frac{mv}{I(t)^2} \frac{dv}{dt} \tag{16}$$

8. INDUCED CURRENT DENSITY

According to Maxwell's first equation, the variable magnetic field generated by the coil generated an azimuthal electric field, resulting in an electromotive force in the superficial layer of the projectile which caused a flow of current.

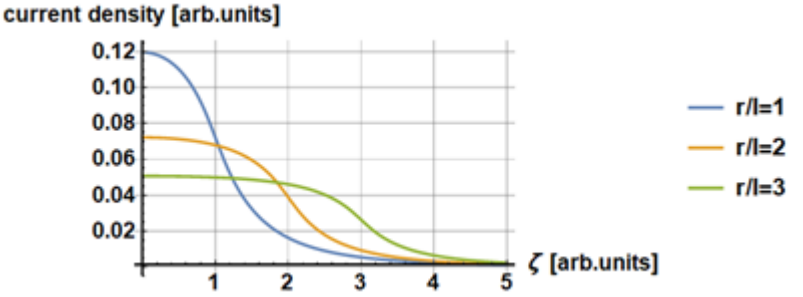

Fig. 6. Axial distribution of current density in the superficial layer of the projectile's material at different radius/length ratios

The electromotive force generated by the magnetic field of the coil was derived from Maxwell's first equation:

$$\int_L E \cdot dl = - \partial\Phi/\partial t$$

$$\Phi = \int_S B_z \cdot dS = 2\pi R^2 \int_0^r B_z(\rho, \zeta, t)\, \rho d\rho \tag{17}$$

Given Ohm's law:

$$E(r,\zeta,t) = \rho_\Omega \cdot j(r, \zeta, t) \tag{18}$$

and formulas (5, 6, and 7), the resulting expression of current density was:

$$j(r, \zeta, t) = \mu_0\, n\, I_0/(\rho_\Omega\, r) \int_0^r h_z(\rho, \zeta, t)\, \rho d\rho \cdot f_2(t) \tag{19}$$

with: ρ_Ω – specific resistance of the projectile's material.

9. PROJECTILE ACCELERATION

The Biot-Savart law facilitated expression of the formula of the electromagnetic force which propelled the projectile:

$$dF_z(\rho,\zeta,t) = B_r(\rho,\zeta,t)\, 2\pi R\rho\, j(\rho,\zeta,t)\, \delta R\, d\zeta \tag{20}$$

The electrodynamic force formula was derived by integrating the foregoing differential expressions within the following limits:

- ρ from 0 to r;
- ζ from ζ_{min} to ζ_{max}, with: ζ_{min} – time-dependent initial position of the projectile (where time dependence means the progress of projectile acceleration); ζ_{max} – relative effective range of electrodynamic force.

Ultimately:

$$F_z(r,t) = 2\pi\mu_0^2\, n^2\, I_0^2\, \omega R\delta/\rho_\Omega \int_{\zeta(t)}^{\zeta_{max}} h_r(r\,\zeta, t) d\zeta \int_0^r h_z(\rho, \zeta, t) d\rho \cdot f_1(t) f_2(t) \tag{21}$$

The momentum input to the projectile was calculated from the equation of momentum and impulse, which facilitated the calculation of the projectile velocity and the projectile's distance in the function of time (and including the balance of momentum):

$$v(t) = \frac{\chi}{m} \int_0^t F_z(r, \zeta,\tau)\, d\tau \tag{22}$$

To fully describe the motion of the projectile, the following equation of distance was required:

$$\zeta(t) = 1/R \int_0^t v(\tau)\, d\tau \tag{23}$$

and the expressions of instantaneous coupling coefficient (14), inductance (11), and kinetic resistance (16). These were the equations which formed a system, the numerical solution of which provided the full data about the progress of the acceleration process, inclusive of the determination of the muzzle velocity and kinetic energy of the projectile and the energy efficiency of the projectile and coil system. Examples of the solution results are given here in Figs. 7 to 10 for a projectile mass of 38 g.

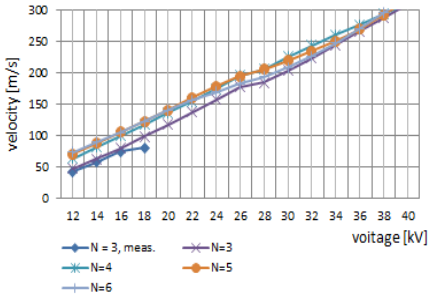

Fig. 7. Muzzle velocity of the projectile

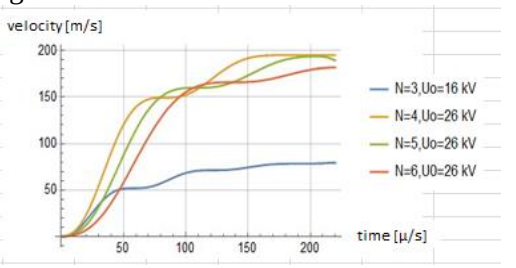

Fig. 8. Projectile velocity vs. time

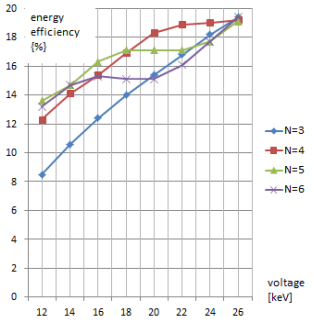

Fig. 9. Energy efficiency

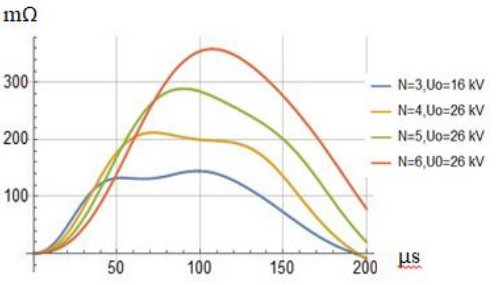

Fig. 10. Kinetic resistance

10. PROJECTILE COMPRESSION

The model presented herein facilitated the calculation of the radial component of electrodynamic force:

$$dF_r(r,\zeta) = B_z(r,\zeta)\, 2\pi R\, r\, j(r,\zeta)\, \delta R\, d\zeta \tag{24}$$

This electrodynamic force applied a compressive pressure to the projectile:

$$p_r(r,\zeta,t) = \mu_0^2\, n^2\, I_0^2\, \omega R\delta/\rho_{Al}\, h_z(r,\zeta,t)/r\int_0^r h_z(\rho,\zeta,t)d\zeta \cdot f_1(t)f_2(t) \tag{25}$$

11. COIL INTERNAL STRESSES

The stresses which occurred in the coil from a high current pulse could be calculated with a formula derived from the Biot-Savart law:

$$p = \mu_o I^2/(2\pi d\phi) \tag{26}$$

with:

p – stress;
I – coil current;
d – coil turn spacing;
φ – wire thickness.

Figure 11 shows examples of plots of the stresses in the coils made from wires of two different thicknesses, with different coil turn spacings and different capacitor bank charging voltages. Given how a suitable composition of e.g. epoxy resin can reach a compression yield stress of approximately 100 MPa, the structure of a coil capable of conducting current surges in excess of 20 kA is perfectly viable.

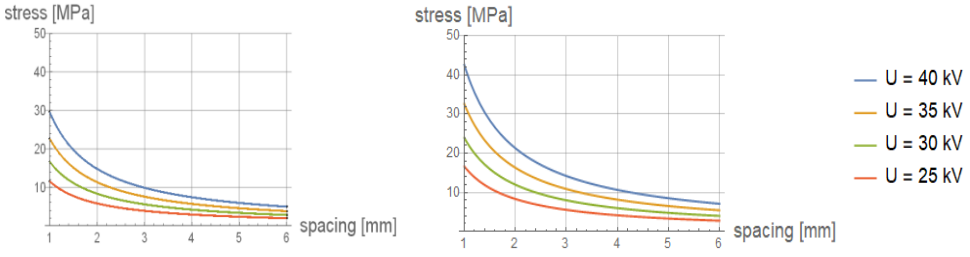

Fig. 11. Stress values within the coil vs. coil turn spacing for different charging voltages of a 12.5 μF capacitor bank, and for two different wire diameters (left: ϕ=2 mm, right: ϕ=3 mm).

12. CASCADE ACCELERATION

The foregoing digital acceleration model facilitated simulating a cascade system comprising multiple driving coils, each of which was a successive acceleration stage of a projectile, by iterative execution of the model code. The muzzle velocity of each acceleration stage was the initial velocity of its successor. An example of the result of the simulation is shown in Fig. 12.

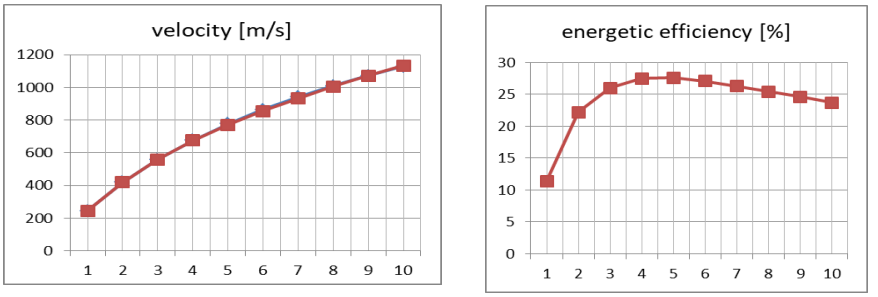

Fig. 12. Muzzle velocity (see the plot to the left) and energy efficiency of the successive stages of the acceleration process (see right) in a cascade system of 10 acceleration stages (coils)

13. CONCLUSION

A major result discussed herein was the plots which corresponded to the number of coil winding layers, 3, see Fig. 7; each pair of plots features a plot of the experimental test result and a plot of the numerical calculations. The experimental test results were in relatively good agreement with the numerical calculation results, which allowed the presented digital model to be treated as reliable (to an extent somewhat limited at the present stage of research). The full reliability of the digital model will be achieved following its confrontation with the acceleration parameters in different coil gun configurations, including a higher number of coil turns, different l/D ratios, different projectile masses, etc. Further evolution of the research into ICG accelerators should combine the development of digital models and experimental testing of successive evolutions of the ICG driving coil.

REFERENCES

[1] Wciślik Mirosław, Tomasz Kwaśniewski. 2006. "Model cylindrycznej cewki jednowarstwowej", *Przegląd Elektrotechniczny* 11 : 1982.
[2] Ingram M.W., J.A. Andrews, D.A. Bresie. 1991. "An Actively Switched Pulsed Induction Accelerator", *IEEE Transactions on Magnetics*, 27(1) : 591-595.
[3] Seog-Whan Kim, Hyun-Kyu Jung, Song-Yop Hahn. 1994. „An Optimal Design of Capacitor-Driven Coilgun", *IEEE Transactions on Magnetics*, 30(2) : 207-211.
[4] Kaye J. Ronald, Gregory A. Mann. 2003. "Reliability Data to Improve High Magnetic Field Coil Design for High Velocity Coilguns", Sandia Report SAND2003-3458.

[5] Kaye J. Ronald. 2005. "Operational Requirements and Issues for Coilgun Electromagnetic Launchers", *IEEE Transactions on Magnetics*, 41(1) : 194-199.

[6] Kaye J. Rachel, B. Turman, M. Aubuchon, Derek C. Lamppa, Geraldine Mann, Edward van Reuth, K. Fulton, Gregory Malejko, P. Magnotti, Dung-Tuan Nguyen, D. Borgwarth, Aylmer Johnson, Ronald Poppe. 2007. Induction Coilgun for EM Mortar. In *Proceedings of 16th IEEE International Pulsed Power Conference*, 1017. 17-22 June 2007, Albuquerque, NM, USA

[7] Yujiao Zhang, Weinan Qin, Junpeng Liao, Jiangjun Ruan, Tao Huang. 2014. "Optimization of Three-stage Electromagnetic Coil Launcher", *Sensors & Transducers* 171(5) : 121-127.

[8] Proceedings of 17th International Symposium on Electromagnetic Launch Technology. 2014. San Diego, California, July 7-11, 2014.

[9] Horodeński Andrzej. 1979. "*Impulsowe grzanie cienkich warstw metalu w układzie rozładowczym z obciążeniem transformatorowym*", oprac. wewn. Instytutu Badań Jądrowych nr 0-148/XXIV/79.

Cyfrowy model procesu elektrodynamicznej akceleracji w urządzeniu typu Coil Gun

Andrzej W. HORODEŃSKI, Cezary POCHRYBNIAK

Narodowe Centrum Badań Jądrowych
ul. Andrzeja Sołtana 7, 05-400 Otwock

Streszczenie. Przedmiotem pracy jest analiza procesu nadawania energii kinetycznej pociskowi wykonanemu z niemagnetycznego materiału przewodzącego, umieszczonemu wewnątrz cewki, przez którą płynie prąd zmienny. Zbudowano model cyfrowy układu akceleracyjnego złożonego z wysokoprądowej cewki oraz umieszczonego wewnątrz niej metalicznego pocisku w kształcie walca. Wykorzystano analityczne wzory na przestrzenny rozkład składowej osiowej i radialnej pola magnetycznego wytwarzanego przez cewkę [5]. Model matematyczny uwzględnia układ przestrzenny cewka-pocisk (wymiary oraz rozkład zwojów cewki), parametry układu zasilającego z uwzględnieniem ich zmienności w czasie spowodowanej przekazem energii do pocisku, w tym zmienność współczynnika sprzężenia, pulsacji, współczynnika tłumienia, indukcyjności i oporności, a także bilans pędu układu cewka-pocisk. Układ równań opisujący układ (prawo indukcji elektromagnetycznej, prawo Biota-Savarta, przemiana energii elektrycznej w kinetyczną, bilans pędu układu cewka-pocisk) rozwiązano metodami numerycznymi. Dokonano eksperymentalnej weryfikacji płynących z analizy wniosków istotnych z punktu widzenia konstrukcji i technologii urządzenia miotającego typu Inductance Coil Gun (ICG). Wykonano wstępne obliczenia mające na celu optymalizację procesu akceleracji. Przeprowadzono także obliczenia wydajności akceleracji w kaskadzie złożonej z 10 cewek.
Słowa kluczowe: Coil Gun, cewka, miotanie, siła elektromagnetyczna